Final Version Available

This preprint is a non peer reviewed version submitted to the Journal of Climate. This work has been accepted for publication with an updated title, *A strong role for the AMOC in partitioning global energy transport and shifting ITCZ position in response to latitudinally discrete solar forcing in the CESM1.2*. The accepted version is substantially different from the preprint version due to the changes and new analysis made during a peer review process. Readers are encouraged to refer to the final version, which is available at https://doi.org/10.1175/JCLI-D-18-0360.1.

Suggested full citation:

Yu, S., and M. Pritchard, 2019: A strong role for the AMOC in partitioning global energy transport and shifting ITCZ position in response to latitudinally discrete solar forcing in the CESM1.2. J. Climate. doi:10.1175/JCLI-D-18-0360.1, in press.

Is oceanic buffering of forced ITCZ shifts controlled by an underappreciated Atlantic meridional overturning circulation pathway?*

Sungduk Yu* and Michael S. Pritchard

Department of Earth System Sciences, University of California, Irvine, California, 92697.

**Corresponding author address:* Department of Earth System Sciences, University of California, Irvine, California, 92697.

E-mail: sungduk@uci.edu

ABSTRACT

Ocean circulation responses to interhemispheric radiative imbalance can damp north-south migrations of the intertropical convergence zone (ITCZ), by reducing the burden on atmospheric heat transport. The role of the Atlantic meridional overturning circulation (AMOC) in such dynamics has not received much attention. Here, we show coupled climate modeling results that suggest AMOC responses are of first order importance to muting ITCZ shift magnitudes as a pair of solar forcing bands is moved from equatorial to polar latitudes. The cross-equatorial energy transport response to the same amount of interhemispheric forcing becomes systematically more ocean-centric when higher latitudes are perturbed in association with strengthening AMOC responses. In contrast, the responses of the Pacific Subtropical Cell are not monotonic and cannot predict this variance in the ITCZ's equilibrium position. Overall these results highlight the importance of the meridional distribution of interhemispheric radiative imbalance and the rich buffering of internal feedbacks that occurs in dynamical versus thermodynamic slab ocean modeling experiments. Mostly, the result implies that the problem of developing a theory of ITCZ migration is entangled with that of understanding the AMOC's response to hemispherically asymmetric radiative forcing—a difficult topic deserving of focused analysis across more climate models.

1. Introduction

The intertropical convergence zone (ITCZ) is a band of intense rainfall encircling most of the tropics, roughly coinciding with the ascending branch of the Hadley Cell. Even a minor shift of its location (or change of its intensity) matters to society as this can result in major fluctuations of regional water availability in the tropics as well as impacting the extratropics through changes in the frequency of tropical cyclones (Dunstone et al. 2013; Merlis et al. 2013) and shifts of the midlatitude jet (Ceppi et al. 2013; Cvijanovic et al. 2013). The zonal-mean position of the ITCZ is largely constrained by interhemispheric energy imbalance of the atmosphere because the thermally-direct Hadley cell transports heat following the direction of its upper branch (i.e. the energetics framework; see Schneider et al. (2014) and Kang et al. (2018) for reviews). That is, the ITCZ resides in the warmer hemisphere so that its upper branch crosses the equator, helping transport heat to the colder hemisphere. Transient ITCZ migrations toward an anomalously warmed hemisphere can occur in response to external forcing over a multitude of timescales, from seasonal to millennial (Donohoe et al. 2013; Schneider et al. 2014).

It is imperative to better understand such ITCZ shift dynamics, and especially the role of the ocean, which has been receiving increased attention. Recent global climate model (GCM) experiments have shown that oceanic dynamics can damp ITCZ shift responses to high-latitude forcing by imposed cloud brightness (Kay et al. 2016), ocean albedo (Hawcroft et al. 2016), sea-ice cover (Tomas et al. 2016), and stratospheric aerosols (Hawcroft et al. 2018). This is in contrast to studies that do not include ocean dynanmics (e.g. Chiang and Bitz 2005; Broccoli et al. 2006; Kang et al. 2008) which exhibit more pronounced ITCZ shifts to extratropical forcings. This occurs since perturbations to interhemispheric energy balance need not be restored by the atmosphere alone in a dynamic ocean coupled GCM; they can also be mediated by changes in oceanic heat transport.

The mechanical coupling between the Hadley cell and the oceanic subtropical cell (STC) via zonal surface wind stress has been attributed to one such damping effect (Held 2001; Schneider et al. 2014; Green and Marshall 2017; Schneider 2017; Kang et al. 2018). But the role of STC damping relative to other potentially important oceanic damping pathways, such as the Atlantic meridional overturning circulation (AMOC), remains unclear. Yet theoretical arguments that the AMOC is fundamental to controlling the annual mean ITCZ location (Frierson et al. 2013; Marshall et al. 2014) motivate its potential importance.

Several modeling studies already suggest important links between the AMOC and the ITCZ position. It has been known for decades that coupled GCM experiments subjected to freshwater hosing in the North Atlantic exhibit southward shifts of the ITCZ in association with a weakened AMOC (Manabe and Stouffer 1995; Vellinga and Wood 2002; Zhang and Delworth 2005; Chang et al. 2008; Zhang et al. 2010; Drijfhout 2010). More recently, Fukar et al. (2013) argued that AMOC-type circulations determine the zonal-mean ITCZ position in an idealized limited-domain coupled GCM. Building on this work, Frierson et al. (2013) and Marshall et al. (2014) showed the ITCZ position's annual mean tendency to lie north of the equator is a result of AMOC heat transport, using a combination of slab ocean aquaplanet and idealized global coupled GCM, along with observational analysis. Other studies allude to an important role of the AMOC in the ITCZ shift response to aerosol clean-up projected over the 21st century. For instance, the projected northward ITCZ shift due to relative warming of the North Atlantic from regional aerosol clean-up is shown to be smaller in the Atlantic than in the Pacific (Rotstayn et al. 2015; Allen 2015) and counteracted by weakening of AMOC (i.e. cooling of the North Atlantic), ultimately muting the shift of annual-mean ITCZ position (AA and Frierson 2017).

The above studies all hint at the potential for ITCZ shifts to be modulated by the AMOC's response to external radiative forcing. But questions remain about how significant this AMOClinked pathway is. Indeed, much is yet to be discovered about how the AMOC responds in general to geographically structured radiative forcing at top of atmosphere, as can occur through latitudinally sensitive cloud feedbacks to climate change, or some volcanoes, or through geoengineering by solar radiation management. Yet this may have implications for ITCZ shift dynamics.

We hypothesize that the AMOC can play an important role for muting ITCZ shift in this context. Conceptually this is based on the fact that on long (greater than interannual) timescales the AMOC variability is driven by thermodynamic forcing (Buckley and Marshall 2016). This is in contrast to wind-driven variations in other circulation components such as the STC, whose variability is mainly driven by mechanical forcing via surface wind stress (JP and Lu 1994; Liu and Philander 1995). A consequence of mechanical coupling in the STC is that the cross-equatorial atmospheric and oceanic energy transports must positively covary (as illustrated in Fig. 1a and b). That is, the partitioning between atmospheric and oceanic responses cannot vary much through the STC coupling, assuming oceanic thermal structures do not change much. The AMOC is not subject to this mechanical constraint; rather its heat transport has the capacity to covary negatively with a given top-of-atmosphere heating imbalance (as illustrated in Fig. 1c and d). Thus, if the AMOC responded sensitively to the details of how a hemispherically asymmetric external forcing were geographically distributed, this could potentially act as an efficient control on ITCZ shift damping efficiency, associated with changes in the overall ocean-atmosphere partitioning of the cross-equatorial energy transport response.

To probe this issue, we present results from a coupled climate model experiment, in which we artificially alter the top-of-atmosphere (TOA) energy budget through solar radiation modulation focused in discrete latitudinal bands at varying distances from the equator (Fig. 2a). The TOA insolation is perturbed to induce a northward heat transport by increasing (decreasing) the solar constant in the southern (northern) hemisphere. Such a perturbation is introduced at four different latitudinal bands (TROP, SUBTROP, MIDLAT, and HIGHLAT) occupying an equal area to examine partitioning responses to the different forcing locations. One additional experiment perturbing the whole hemisphere at a quarter of the magnitude (i.e. identical interhemispheric power asymmetry) is also performed (WHOLE). TOA forcing allows freedom for the simulated climate system to internally select its preferred partitioning of heat transport responses between the atmosphere and ocean (and, within the ocean, between AMOC vs. other ocean circulation components). Our forcing is in some ways similar to Mechoso et al. (2016) (solar flux alteration) and Haywood et al. (2016); Hawcroft et al. (2018) (stratospheric aerosol management), but also with three notable differences—(i) we only perturb non-UV part of solar radiation to avoid a direct stratospheric perturbation, (ii) we avoid net global perturbation by introducing both solar flux source and sink, and (iii) we integrate for long enough to sample AMOC responses (200 years, compared to 20 (Haywood et al. 2016), 25 (Mechoso et al. 2016), and 80 (Hawcroft et al. 2018) years).

Consistent with our hypothesis, the results will reveal a strong correlation between the magnitude of AMOC responses and the meridional distribution of interhemispheric forcing, which in turn explains a large degree of variance in the degree of ITCZ shift response that occurs at equilibrium.

2. Method

a. GCM simulations

The Community Earth System Model (CESM) version 1.2.2. (Hurrell et al. 2013) is used, configured with interactive atmosphere, land, ocean and sea ice components in a preindustrial experiment mode initialized with a spun-up ocean (i.e. the standard "B_1850_CAM5" component set). A set of five experiments that induce interhemispheric energy imbalance at top of the simulated atmosphere (TOA), but in different latitude ranges, by dividing each hemisphere into four zonal bands of equal area, eg. tropical, subtropical, mid-latitude, and high-latitude zones. The four experiments are called TROP, SUBTROP, MIDLAT and HIGHLAT hereafter. In addition, we perform an extra experiment (WHOLE) of which the whole hemisphere is perturbed but at a quarter magnitude in order to keep the area-integrated perturbation identical to other cases. A control simulation (CTRL) is conducted with no perturbation for the same period as experimental simulations. In each test, we introduce an artificial incoming non-UV shortwave energy source / sink pair at the TOA in the southern / northern hemisphere, of magnitude 17 W m^{-2} in annual mean—by multiplying a constant factor, not adding, in order to prevent exceedingly high perturbation during winter. Our decision to position our forcing at TOA is attractive philosophically as it maximizes the simulated climate system's freedom to excite internal feedbacks and to internally select the partitioning of the meridional energy transport response between atmosphere and ocean. Each simulation is integrated for 200 years, but the last 150 years of simulations are used for the analysis in this paper, unless otherwise noted. Model simulation output and model code modification are available upon request.

b. Meridional energy transport calculation

The total (atmospheric plus oceanic) meridional heat transport, F, is calculated as

$$F(\phi) = -\int_{\phi}^{\pi/2}\int_{0}^{2\pi}\left[R_{TOA} - \frac{\partial(E_A)}{\partial t} - \frac{\partial(E_O)}{\partial t}\right]a^2 cos\phi d\theta d\phi,$$

where R_{TOA} is a residual radiative flux at TOA, E_A (E_O) is a column energy storage of atmosphere (ocean), a is the Earth radius, and θ and ϕ are longitude and latitude, respectively. Zonally-integrated meridional oceanic heat transport, F_O, is directly calculated from the ocean model by summing advective and diffusive fluxes over depth and longitude at each latitude. Meridional atmospheric heat transport, F_A, is calculated as a residual, e.g. $F_A = F - F_O$.

c. Oceanic heat transport decomposition

Cross-equatorial OHT is decomposed into into its dynamic ($T_{ctrl}\Delta \upsilon$), thermodynamic ($\upsilon_{ctrl}\Delta T$), and nonlinear components ($\Delta \upsilon \Delta T$),

$$\Delta(\upsilon T) = T_{ctrl}\Delta \upsilon + \upsilon_{ctrl}\Delta T + \Delta \upsilon \Delta T,$$

where υ is meridional velocity, T is temperature, $\Delta(\cdots) = (\cdots)_{exp} - (\cdots)_{ctrl}$, and subscript exp (ctrl) means experiment (control) simulation result.

d. Tropical precipitation asymmetry index (PAI)

Following Hwang and Frierson (2013), precipitation asymmetry index is calculated as the area-weighted mean precipitation rate difference between north (0° to 20°N) and south (20°S to 0°), then normalized by the area-weighted mean precipitation rate of the whole tropics (20°S to 20°N). Accordingly, the PAI captures the relative strength of the two solstice season ITCZ positions, as which we define the position of *annual-mean* ITCZ. The responses of PAI are well-correlated with that of the tropical precipitation centroid (Fig. S1), which is another popular measure of annual-mean ITCZ position.

3. Results

We begin by analyzing the annual-mean ITCZ precipitation response across the experiment ensemble using the last 150-year average. A southward ITCZ "shift", a term we will use as shorthand to describe an increase (decrease) in intensity of the southern (northern) zonal-mean, annual-mean rainfall band, is observed in all cases, as expected by the northward cross-equatorial atmospheric heat transport (AHT) response to warming (cooling) the southern (northern) hemisphere. However, its magnitude monotonically decreases as the forcing bands are moved poleward (Fig. 2b). This differing ITCZ shift response occurs *despite* the fact that the magnitude of incoming solar forcing asymmetry is constrained to be identical across the experiments. This implies that either (i) latitudinally varying internal radiative feedbacks modify the effective magnitude of the asymmetric forcing across experiments; and/or (ii) the cross-equatorial oceanic heat transport (OHT) response is sensitive to the geographic details of the forcing. While the effective forcing (i.e. including radiative feedbacks), which mostly determines the cross-equatorial total heat transport since oceanic heat content change is very small (Fig. 3), does show some variation across experiments, there is remarkably little spread in its net interhemispheric asymmetry (Fig. 2b) with a range of 2.90–3.38 W m^{-2} as a result of compensating internal radiative feedbacks (Fig. 3). This is interestingly inconsistent with the results of Seo et al. (2014), in which latitudinally sensitive cloud feedbacks are able to exert strong control of AHT due to the use of a slab ocean model; the implication is that dynamic oceanic buffering is important to this issue. For our own purposes the main point is that such internal radiative feedback can only explain about 0.12 PW spread in the total (oceanic plus atmospheric) cross-equatorial heat transport response, arguing against (i). In contrast the spread of AHT alone is much larger (Fig. 2c), implying that variability in the annual-mean ITCZ shift response is mainly driven by variability in OHT responses across the experiments.

So far we have found that the cross-equatorial heat transport partitioning between ocean and atmosphere becomes a key factor that determines the magnitude of ITCZ shift in our experiments: When interhemispherically asymmetric solar forcing is concentrated at higher latitudes, the partitioning of the coupled response becomes more ocean-centric and thus the ITCZ shift response becomes more muted. The question naturally arises as to why.

Before proceeding, we first confirm that it is appropriate to view relationships between AHT and ITCZ across our experiments through an energetics framework. This acknowledges that there can be special cases where such a framework can be inappropriate, for instance if the heat transport efficiency of the Hadley circulation (i.e. the gross moist stibility, GMS) dominates spread in the AHT response (Seo et al. 2017) or if the eddy heat transport dominates spread in the time mean Hadley circulation heat transport (Roberts et al. 2016). However, in our case, the cross-equatorial AHT response is a good proxy for a zonal-mean ITCZ shift response. A tight linear relationship between the cross-equatorial AHT and the mean meridional circulation (Hadley circulation) responses show GMS responses are secondary (Fig. 4), and the eddy heat transport (transient plus stationary) responses are much weaker than Hadley cell heat transport and scale with the strength of Hadley circulation (Fig. 5). Thus a time-mean energetics framework is appropriate to apply in our analysis.

Fig. 6 shows that Atlantic dynamics play a leading role in driving the tendency towards a more ocean-centric energy transport response with higher latitude forcing. To understand the role of each ocean, the basin-specific OHT responses are decomposed into dynamic and thermodynamic components (Fig. 6). The OHT responses to changing the latitudinal position of hemispherically asymmetric forcing are mostly driven by dynamic changes, not thermodynamic. But different ocean basins respond differently. Only the Atlantic shows a clear monotonic sensitivity across experiments in line with the global OHT sensitivity. In contrast, the Pacific-Indian OHT does not exhibit a monotonic sensitivity, except during the transition from SUBTROP to MIDLAT, during which both Atlantic and Pacific-Indian basins show comparable OHT increases. Despite the fact that the absolute magnitude of the Atlantic OHT response is generally smaller than that of the Pacific-Indian, normalized by its respective basin width the Atlantic is a much more efficient energy transporter (yellow dots in Fig. 6) and seems to play a controlling role in the experiments.

This draws our analysis toward the Atlantic meridional overturning circulation (AMOC), as the main dynamical pathway of meridional oceanic heat transport in the Atlantic. Consistent with the Atlantic OHT, the AMOC response becomes monotonically stronger as the solar forcing bands are moved poleward (Fig. 7a). Transient analysis shows this monotonic sorting with forcing latitude emerges within 30 years (Fig. 8a) and persists for two centuries amidst internal variability. There is reassuring consistency in the unsteady evolution of the anomalous Atlantic OHT and AMOC strength (Fig. 8a and b).

Unlike the AMOC responses, the Pacific-Indian STC responses do not exhibit a monotonic sensitivity with implications for total cross-equatorial OHT (Fig. 8c). While tantalizing changes in the STC circulation response do occur (Fig. 7b, and hemispherically asymmetric component in Fig. S2), no associated cross-equatorial OHT responses are detectable (Fig. 8d). This implies internal compensations in the structure of the shallow overturning circulation's response buffer its overall interhemispheric energetics. The buffering mechanisms are case specific. For instance, in HIGHLAT, despite the fact that a weakening of the STC mass circulation response might act to reduce its OHT relative to CTRL, this is compensated by a deepening of the circulation indicating increasing vertical thermal contrast—in turn implying more efficient heat transport per unit overturning circulation, thus acting to increase OHT in resistance to the weaker circulation. A separate mechanism buffers the TROP experiment, via spinup of a strong cross-equatorial roll-type circulation near the equator (Miyama et al. 2003) that acts against weakened STC mass circulation, in this case through a mechanism that is independent of the STC's depth.

Different timescale between Pacific and Atlantic Mechanism

In Fig. 9, scatter plots of key predictors of tropical precipitation asymmetry both within experiments (i.e. dots of one color) and across experiments (i.e. dots spanning multiple colors) provide an especially compact way to contrast the differing roles of the two ocean basins on multidecadal (top) vs. interannual (bottom) timescales. On long timescales, the decomposition of the global relationship between PAI and OHT shows that the Atlantic clearly controls the equilibrium state response to the TOA forcing (monotonic color ranking along statistically significant inter-experiment regression line in Fig. 9a, b), whereas the Pacific-Indian OHT cannot detectably predict global PAI variance within noise (Fig. 9c). However, on short timescales, a robust regression is detected within each experiment between Pacific-Indian OHT and global PAI (colored regression lines in Fig. 9d, f). This timescale separation between the two ocean basins is robust to variations of the exact running mean windows used to discriminate short- from long-term behavior, although the long-term Atlantic correlation reaches its maximum around a 10-year averaging window (Fig. 9g).

The opposite signs of the PAI–OHT correlation for the Atlantic (across experiments) versus the Pacific-Indian (within experiments) illustrate the fundamental difference of AMOC vs. STC freedom to damp ITCZ shifts that was alluded to in the introduction and Fig. 1. Keeping in mind that a more negative PAI implies a more southward ITCZ position and a more positive (northward) cross-equatorial AHT (Fig. 10), the regressions in Fig. 9 show that Atlantic OHT negatively covaries with AHT, whereas Pacific-Indian OHT positively covaries with AHT. This confirms our hypothesis that an AMOC response has the capacity to be an efficient ITCZ shift damping mechanism, as it can significantly alter the partitioning between atmospheric and oceanic heat transport.

We note that the cross-experiment correlation between the PAI and the Atlantic OHT_{eq} responses (Fig. 9b) does not depend on the fact that the magnitude of effective forcing (forcing + radiative feedbacks)—which dictates the total heat transport (TotalHT) magnitude—happens to have been similar across our experiments (e.g. Fig. 2c). While the response magnitudes of ΔAHT_{eq} and

ΔOHT_{eq} are constrained by the effective forcing magnitude ($\Delta AHT_{eq} + \Delta OHT_{eq} = \Delta TotalHT_{eq}$), the *partitioning* between ΔAHT_{eq} and ΔOHT_{eq} is not, i.e.

$$\frac{\Delta AHT_{eq}}{\Delta TotalHT_{eq}} + \frac{\Delta OHT_{eq}}{\Delta TotalHT_{eq}} = 1, \tag{1}$$

implying that the negative covariance between the normalized quantities is guaranteed despite the fact that the covariance of the un-normalized quantities depends on the magnitude of $\Delta TotalHT_{eq}$. Assuming that the Hadley Circulation heat transport dominates the cross-equatorial atmospheric heat transport ($\Delta AHT_{eq} = \Delta AHT_{eq}^{HC} + \Delta AHT_{eq}^{EDDY} \approx \Delta AHT_{eq}^{HC}$; Fig. 5), that the cross-equatorial oceanic heat transport is mostly driven by two overturning circulations ($\Delta OHT_{eq} \approx \Delta OHT_{eq}^{STC} + \Delta OHT_{eq}^{AMOC}$), and that AHT_{eq}^{HC} and OHT_{eq}^{STC} are coupled ($\Delta OHT_{eq}^{STC} \approx \alpha \Delta AHT_{eq}^{HC}$; Held (2001)), Eq. 1 can be simplified to

$$(1+\alpha)\frac{\Delta AHT_{eq}^{HC}}{\Delta TotalHT_{eq}} + \frac{\Delta OHT_{eq}^{AMOC}}{\Delta TotalHT_{eq}} = 1, \tag{2}$$

where the superscripts HC, EDDY, STC, and AMOC denote heat transport components due to the Hadley Circulation, eddies, the subtropical cell, and the Atlantic meridional circulation, respectively, and α is a positive definite function. Accordingly, we expect to see a similarly tight, if not tighter, correlation when normalizing OHT_{eq} by the effective forcing magnitude; indeed this is confirmed in Fig. S3.

4. Discussion

The many internal feedbacks in our experiments have led to behaviors worth contrasting against the intuition gained from slab ocean modeling setups, which would not have predicted them. For instance, using a slab-ocean coupled GCM forced by a prescribed oceanic heat transport, Seo et al. (2014) showed amplifying TOA energy imbalance and hence a larger ITCZ shift with higher latitude perturbation, and explained this as a result of net positive SST–low cloud, SST–outgoing longwave radiation (OLR) feedbacks. Despite the fact that similar SST-mediated radiative feedbacks also exist in our study, we observe a TOA energy imbalance that is largely insensitive to forcing latitude. This can be traced to the fact that we observe a much weaker SST response magnitude (Fig. 11a) in our more heavily buffered system. For instance, our SST response for HIGHLAT is about 3 K, but this is an order of magnitude smaller than Seo el al. (20–80 K) despite the fact that their forcing magnitude is only 1.64 times larger than in our experiment. A decomposition of the details shows that for our high latitude forcing cases (MIDLAT and HIGHLAT), the SST–OLR negative feedback actually wins over the positive SST-low cloud feedback. This underscores that important positive feedbacks that were not included in the setup of Seo et al. (2014) ended up playing leading roles in our high latitude forcing cases (Fig. 3). One likely culprit is the positive ice–albedo feedback, which counteracts the negative SST–OLR feedback. It is unclear whether the resilient net TOA response across our simulations is a coincidence, or an intrinsic feature of the Earth's climate system in the limit of fully interactive radiative/convective/SST feedbacks; this could be worth more study. Regardless, our findings about partitioning do not depend on the net TOA response magnitude having turned out this way (Fig. 9 and Fig. S3).

Meanwhile, the damped SST response in our simulations highlights the importance of the ocean circulation's role in the global energy budget. Ocean dynamics limit excessive local storage of heat near the surface by redistributing it vertically and horizontally. We have focused on the striking role of overturning circulations in this regard, but the role of gyre circulations would also be an interesting direction for future work to further understand the ocean's role in ITCZ shift buffering. While the subtropical gyre circulations do not participate much in the direct (advective) heat exchange across the equator, they can non-locally affect both the atmospheric and oceanic column energy budgets via SST-dependent feedbacks, such as through SST–low cloud feedbacks modulated by gyre currents that carry anomalously heated surface water away from radiative action centers (Mechoso et al. 2016). Indeed, such linkages occur in our experiments (Fig. 11).

It is worth commenting on the utility of using a theoretical framework pinned on equatorial atmospheric net energy input ($\mathrm{NEI_{eq}}$) to interpret our simulations. $\mathrm{NEI_{eq}}$ has been argued to determine the sensitivity of the latitude of the zonal-mean ITCZ (ϕ_{ITCZ}) to a given magnitude of $\mathrm{AHT_{eq}}$ perturbation, i.e. $\phi_{\mathrm{ITCZ}} \sim \frac{\mathrm{AHT_{eq}}}{\mathrm{NEI_{eq}}}$ (Bischoff and Schneider 2014). $\mathrm{NEI_{eq}}$ is also known to correlate with the hemispherically symmetric component of tropical precipitation biases including the double ITCZ bias (Adam et al. 2016, 2017). We hypothesize that variations in the $\mathrm{NEI_{eq}}$ response to solar forcing do not play a leading role in our experiments based on the quasi-linear relationship between interannual PAI vs. global $\mathrm{OHT_{eq}}$ responses (Fig. 9d, f). Consistent with this view, the fractional response of $\mathrm{NEI_{eq}}$ is much smaller than that of $\mathrm{AHT_{eq}}$ (Fig. 12). However, we acknowledge that effects of $\mathrm{NEI_{eq}}$ are important and may be responsible for the deviation from the linear regression line, since changes in $\mathrm{NEI_{eq}}$ can cause ITCZ shifts independent of changes in $\mathrm{AHT_{eq}}$.

An obvious limitation of this study is the use of a single climate model, which raises the question of whether similar responses should be expected in other climate models. On the one hand, a satisfying answer on inter-model spread will only be gleaned from focused intercomparison, which will be forthcoming via a new Extratropical-Tropical Interaction Model Intercomparison Project. This community activity will include analysis of atmosphere-ocean partitioning of the energy transport response to extratropical TOA perturbation [Sarah Kang, personal communication, 2017]. On the other hand, it is also already logical to expect some degree of similar responses to occur across independent models. Despite the fact that the temporal mean structure and variability of the AMOC varies widely among Coupled Model Intercomparison Project version 3 and 5 (CMIP3 and 5) models (Medhaug and Furevik 2011; Zhang and Wang 2013; Muir and Fedorov 2015), the AMOC's response to differing forms of radiative forcing tends to share a common sign.

Across CMIP5 models, anthropogenic CO_2 forcing tends to weaken the AMOC (Gregory et al. 2005; Cheng et al. 2013), and volcanic aerosol forcing strengthens it (Ding et al. 2014) while also shifting the ITCZ towards the hemisphere opposite to eruption (Iles and Hegerl 2014). Anthropogenic aerosol forcing has also been shown to strengthen the AMOC across a set of independent studies that used different coupled GCMs (e.g. GFDL CM2.1 (Delworth and Dixon 2006), CSIRO Mk2.1 (Cowan and Cai 2013), and HadGEM2-ES (Menary et al. 2013)). Especially considering that our TOA solar perturbation shares some similarities to a geographically confined aerosol radiative forcing, these are all reasons to expect the sensitivity we have shown in CESM should be detectable in other CMIP5-class climate models.

Another limitation of this work is that it does not attempt to fully attribute the mechanistic pathway connecting regional TOA solar forcing to varying degrees of AMOC response. While beyond scope, we view it as an interesting topic worthy of future work, via process analysis focused on subducting regions. As expected from cooling of the North Atlantic, positive regional anomalies of surface ocean density over the Labrador Sea deep water formation region lead AMOC responses in all our experiments (Fig. 13). But the origin of these density perturbations in the Labrador Sea is not immediately obvious, especially in the case of low-latitude forcing experiments where solar perturbations are applied away from the deep water formation regions. Relevant processes are likely to include advection of buoyancy anomalies through subtropical and subpolar gyres and regional meteorological changes via tropical-extratropical teleconnection. Future work focusing on these mechanistic process chains might help contribute to further understanding of the AMOC–ITCZ nexus. Another caveat of our experimental design is that the TROP forcing somewhat awkwardly attempts to force a sharp thermal gradient near the equator. On the one hand, the actual near-equatorial SST gradient response of this subexperiment is not an outlier relative to our other simulations, which suggests sharp thermal gradients are efficiently buffered by dynamics that must resist them near the equator (Fig. 14). Nonetheless, future iterations of this experiment design would benefit from avoiding this technical issue.

A final limitation is our use of idealized, geographically localized forcing bands to probe the coupled system's dynamics. It is natural to wonder to what degree this informs understanding of the system's sensitivity to more realistic sources of interhemispherically asymmetric solar forcing like volcanoes or geo-engineering. In this context we suggest it may be possible to think of our experiments as akin to Green?s functions, or kernels, in that they have some demonstrable additive utility. That is, the results of the WHOLE experiment, in which we perturb each entire hemisphere at one quarter the power magnitude of the four regional sub-experiments, reproduces to a remarkable degree the linear average of those four experiments' independent responses (e.g. Figs. 6, 7, and 3). This implies some generality beyond our idealized setup that could be practically relevant to many realistic forcing contexts; the idea of kernels summarizing these dynamics is worth exploring more.

Notwithstanding such limitations, one implication of our results relates to improving tropical rainfall biases in coupled GCMs. Our results, along with recent coupled GCM studies (Kay et al. 2016; Hawcroft et al. 2016, 2018), seem to challenge the notion that *high-latitude* cloud radiative biases play a controlling role on biases of tropical precipitation, a view that has been supported by correlations across CMIP5 models(Hwang and Frierson 2013). Our experiments imply the opposite, given that the AMOC response can provide an efficient buffer to ITCZ shifts when hemispherically asymmetric radiative forcing biases are concentrated at high latitudes. The reduction of this oceanic buffering pathway when the same interhemispheric forcing is focused at low latitudes implies that even a small bias in cloud radiative forcing near the tropics might induce a strong atmospheric (ITCZ shift) response. This appears consistent with the findings of Xiang et al. (2017) who argued that across CMIP5 models, the degree of the double ITCZ bias of coupled models is better predicted by the hemispheric asymmetry of their net TOA shortwave fluxes near the tropics in atmosphere-only simulations, than by those in the extratropics. It also evokes the findings of Mechoso et al. (2016) who showed stratocumulus cloud biases in the subtropics can overwhelm modifications to southern ocean radiative forcing. Together, these results support renewed focus on improving *low-latitude* radiation biases towards improving tropical precipitation.

5. Conclusion

We have shown results from a comprehensive global climate model that reveals the AMOC can be especially important in setting the degree to which ocean dynamics act to damp radiatively forced migrations of the zonal-mean ITCZ. This effect becomes strong when an interhemispherically asymmetric forcing is focused at high latitudes, highlighting the importance of the meridional distribution of shortwave radiative forcing in such dynamics. The main implication is that ongoing attempts to develop ITCZ migration theory that includes the role of buffering by ocean dynamics may ultimately depend on a satisfying theory for the AMOC's response to radiative forcing, and its links to the ITCZ. Another practical implication for near-term GCM development is that fixing low-latitude TOA radiative biases in climate models might be a more practical strategy towards improving tropical rainfall biases than fixing high-latitude biases.

Acknowledgments. We would like to acknowledge François Primeau for helpful discussions. This work was funded by National Science Foundation AGS-1419518. Model simulations were done in Yellowstone (ark:/85065/d7wd3xhc) provided by NCAR's CISL, sponsored by the National Science Foundation.

BibTeX. It uses references.bib and the ametsoc2014.bst file for the style.

References

AA, M., and D. W. Frierson, 2017: The role of ocean fluxes and radiative forcings in determining tropical rainfall shifts in RCP8.5 simulations. *Geophysical Research Letters*, doi:10.1002/2017GL074473.

Adam, O., T. Schneider, and F. Brient, 2017: Regional and seasonal variations of the double-ITCZ bias in CMIP5 models. *Clim. Dyn.*, 1–17, doi:10.1007/s00382-017-3909-1.

Adam, O., T. Schneider, F. Brient, and T. Bischoff, 2016: Relation of the doubleITCZ bias to the atmospheric energy budget in climate models. *Geophys Res Lett*, doi:10.1002/2016GL069465.

Allen, R. J., 2015: A 21st century northward tropical precipitation shift caused by future anthropogenic aerosol reductions. *Journal of Geophysical Research: Atmospheres*, doi:10.1002/2015JD023623.

Bischoff, T., and T. Schneider, 2014: Energetic constraints on the position of the intertropical convergence zone. *Journal of Climate*, **27 (13)**, 4937–4951, doi:10.1175/JCLI-D-13-00650.1.

Broccoli, A., K. Dahl, and R. Stouffer, 2006: Response of the ITCZ to northern hemisphere cooling. *Geophys. Res. Lett.*, **33**, L01 702, doi:10.1029/2005GL024546.

Buckley, M., and J. Marshall, 2016: Observations, inferences, and mechanisms of the atlantic meridional overturning circulation: A review. *Rev. Geophys.*, **54**, 5–63, doi:10.1002/2015RG000493.

Ceppi, P., Y. Hwang, X. Liu, D. M. Frierson, and D. L. Hartmann, 2013: The relationship between the ITCZ and the southern hemispheric eddydriven jet. *J Geophys Res Atmospheres*, **118 (11)**, 5136–5146, doi:10.1002/jgrd.50461.

Chang, P., and Coauthors, 2008: Oceanic link between abrupt changes in the north atlantic ocean and the african monsoon. *Nature Geoscience*, **1 (7)**, 444–448, doi:10.1038/ngeo218.

Cheng, W., J. C. H. Chiang, and D. Zhang, 2013: Atlantic meridional overturning circulation (AMOC) in CMIP5 models: RCP and historical simulations. *Journal of Climate*, **26 (18)**, 7187–7197, doi:10.1175/JCLI-D-12-00496.1.

Chiang, J. C., and C. M. Bitz, 2005: Influence of high latitude ice cover on the marine intertropical convergence zone. *Clim Dynam*, **25 (5)**, 477–496, doi:10.1007/s00382-005-0040-5.

Cowan, T., and W. Cai, 2013: The response of the largescale ocean circulation to 20th century asian and nonAsian aerosols. *Geophys Res Lett*, **40 (11)**, 2761–2767, doi:10.1002/grl.50587.

Cvijanovic, I., P. L. Langen, E. Kaas, and P. D. Ditlevsen, 2013: Southward intertropical convergence zone shifts and implications for an atmospheric bipolar seesaw. *J Climate*, **26 (12)**, 4121–4137, doi:10.1175/JCLI-D-12-00279.1.

Delworth, T. L., and K. W. Dixon, 2006: Have anthropogenic aerosols delayed a greenhouse gas-induced weakening of the north atlantic thermohaline circulation? *Geophys. Res. Lett.*, **33 (2)**, doi:10.1029/2005GL024980.

Ding, Y., J. A. Carton, G. A. Chepurin, G. Stenchikov, A. Robock, L. T. Sentman, and J. P. Krasting, 2014: Ocean response to volcanic eruptions in coupled model intercomparison project 5 simulations. *J. Geophys. Res. Ocean*, **119 (9)**, 5622–5637, doi:10.1002/2013JC009780.

Donohoe, A., J. Marshall, and D. Ferreira, 2013: The relationship between ITCZ location and cross-equatorial atmospheric heat transport: From the seasonal cycle to the last glacial maximum. *Journal of Climate*.

Drijfhout, S. S., 2010: The atmospheric response to a thermohaline circulation collapse: Scaling relations for the hadley circulation and the response in a coupled climate model. *J Climate*, **23 (3)**, 757–774, doi:10.1175/2009JCLI3159.1.

Dunstone, N., D. Smith, B. Booth, L. Hermanson, and R. Eade, 2013: Anthropogenic aerosol forcing of atlantic tropical storms. *Nat Geosci*, **6 (7)**, 534–539, doi:10.1038/ngeo1854.

Frierson, D. M. W., and Coauthors, 2013: Contribution of ocean overturning circulation to tropical rainfall peak in the northern hemisphere. *Nat. Geosci*, **6**, doi:10.1038/ngeo1987.

Fukar, N. S., S. Xie, R. Farneti, E. A. Maroon, and D. M. Frierson, 2013: Influence of the extratropical ocean circulation on the intertropical convergence zone in an idealized coupled general circulation model. *J. Climate*, **26 (13)**, 4612–4629, doi:10.1175/JCLI-D-12-00294.1.

Green, B., and J. Marshall, 2017: Coupling of trade winds with ocean circulation damps ITCZ shifts. *J Climate*, doi:10.1175/JCLI-D-16-0818.1.

Gregory, J., and Coauthors, 2005: A model intercomparison of changes in the atlantic thermohaline circulation in response to increasing atmospheric CO2 concentration. *Geophys. Res. Lett.*, **32 (12)**, L12 703, doi:10.1029/2005GL023209.

Hawcroft, M., J. Haywood, M. Collins, and A. Jones, 2016: Southern ocean albedo, interhemispheric energy transports and the double ITCZ: global impacts of biases in a coupled model. *Climate Dynamics*, doi:10.1007/s00382-016-3205-5.

Hawcroft, M., J. M. Haywood, M. Collins, and A. Jones, 2018: The contrasting climate response to tropical and extratropical energy perturbations. *Climate Dynamics*, doi:10.1007/s00382-018-4076-8.

Haywood, J. M., and Coauthors, 2016: The impact of equilibrating hemispheric albedos on tropical performance in the HadGEM2 ES coupled climate model. *Geophys. Res. Lett.*, **43 (1)**, 395–403, doi:10.1002/2015GL066903.

Held, I., 2001: The partitioning of the poleward energy transport between the tropical ocean and atmosphere. *Journal of the atmospheric sciences*, doi:10.1175/1520-0469(2001)058⟨0943:TPOTPE⟩2.0.CO;2.

Hurrell, J. W., and Coauthors, 2013: The community earth system model: A framework for collaborative research. *Bulletin of the American Meteorological Society*, **94 (9)**, 1339–1360, doi:10.1175/BAMS-D-12-00121.1.

Hwang, Y., and D. Frierson, 2013: Link between the double-Intertropical convergence zone problem and cloud biases over the southern ocean. *Proceedings of the National* , **10 (13)**, 4935–4940, doi:10.1073/pnas.1213302110.

Iles, C., and G. Hegerl, 2014: The global precipitation response to volcanic eruptions in the CMIP5 models. *Environmental Research Letters*, **9**, 104 012 (10pp).

JP, M., and P. Lu, 1994: Interaction between the subtropical and equatorial ocean circulations: The subtropical cell. *Journal of Physical Oceanography*, **24**, 466–497, doi:10.1175/1520-0485(1994)024⟨0466\:IBTSAE⟩2.0.CO.

Kang, S., I. Held, D. Frierson, and M. Zhao, 2008: The response of the ITCZ to extratropical thermal forcing: Idealized slab-ocean experiments with a GCM. *Journal of Climate*.

Kang, S. M., Y. Shin, and S. Xie, 2018: Extratropical forcing and tropical rainfall distribution: energetics framework and ocean ekman advection. *npj Climate and Atmospheric Science*, **1 (1)**, doi:10.1038/s41612-017-0004-6.

Kay, J. E., C. Wall, V. Yettella, B. Medeiros, C. Hannay, P. Caldwell, and C. Bitz, 2016: Global climate impacts of fixing the southern ocean shortwave radiation bias in the community earth system model (CESM). *Journal of Climate*, **29 (12)**, 4617–4636, doi:10.1175/JCLI-D-15-0358.1.

Liu, Z., and S. G. H. Philander, 1995: How different wind stress patterns affect the tropical-subtropical circulations of the upper ocean. *Journal of physical oceanography*, doi:10.1175/1520-0485(1995)025⟨0449:HDWSPA⟩2.0.CO;2.

Manabe, S., and R. Stouffer, 1995: Simulation of abrupt climate change induced by freshwater input to the north atlantic ocean. *Nature*, **378**.

Marshall, J., A. Donohoe, D. Ferreira, and M. D, 2014: The ocean's role in setting the mean position of the Inter-Tropical convergence zone. *Climate Dynamics*, **42**, 1967–1979, doi:10.1007/s00382-013-1767-z.

Mechoso, C., and Coauthors, 2016: Can reducing the incoming energy flux over the southern ocean in a CGCM improve its simulation of tropical climate? *Geophys Res Lett*, **43 (20)**, doi:10.1002/2016GL071150.

Medhaug, I., and T. Furevik, 2011: North atlantic 20th century multidecadal variability in coupled climate models: sea surface temperature and ocean overturning circulation. *Ocean Sci.*, **7 (3)**, 389–404, doi:10.5194/os-7-389-2011.

Menary, M., and Coauthors, 2013: Mechanisms of aerosolforced AMOC variability in a state of the art climate model. *Journal of* , **118**, 2087–2096, doi:10.1002/jgrc.20178.

Merlis, T. M., M. Zhao, and I. M. Held, 2013: The sensitivity of hurricane frequency to ITCZ changes and radiatively forced warming in aquaplanet simulations. *Geophys Res Lett*, **40 (15)**, 4109–4114, doi:10.1002/grl.50680.

Miyama, T., M. Julian, T. Jensen, J. Loschnigg, S. Godfrey, and A. Ishida, 2003: Structure and dynamics of the Indian-Ocean cross-equatorial cell. *Deep Sea Res Part Ii Top Stud Oceanogr*, **50 (12-13)**, 2023–2047, doi:10.1016/S0967-0645(03)00044-4.

Muir, L., and A. Fedorov, 2015: How the AMOC affects ocean temperatures on decadal to centennial timescales: the north atlantic versus an interhemispheric seesaw. *Clim Dynam*, **45 (1-2)**, 151–160, doi:10.1007/s00382-014-2443-7.

Roberts, W. G., P. Valdes, and J. Singarayer, 2016: Can energy fluxes be used to interpret glacial/interglacial precipitation changes in the tropics? *Geophys. Res. Lett.*, **44**, 63736382, doi:10.1002/2017GL073103.

Rotstayn, L., M. Collier, and J. Luo, 2015: Effects of declining aerosols on projections of zonally averaged tropical precipitation. *Environmental Research* , **10**, 044 018, doi:10.1088/1748-9326/10/4/044018.

Schneider, T., 2017: Feedback of AtmosphereOcean coupling on shifts of the intertropical convergence zone. *Geophysical Research Letters*, doi:10.1002/2017GL075817.

Schneider, T., T. Bischoff, and G. Haug, 2014: Migrations and dynamics of the intertropical convergence zone. *Nature*, doi:10.1038/nature13636.

Seo, J., S. Kang, and D. Frierson, 2014: Sensitivity of intertropical convergence zone movement to the latitudinal position of thermal forcing. *J Climate*, **27 (8)**, 3035–3042, doi:10.1175/JCLI-D-13-00691.1.

Seo, J., S. Kang, and T. Merlis, 2017: A model intercomparison of the tropical precipitation response to a CO2 doubling in aquaplanet simulations. *Geophysical Research Letters*, 993–1000, doi:10.1002/2016GL072347.

Tomas, R. A., C. Deser, and L. Sun, 2016: The role of ocean heat transport in the global climate response to projected arctic sea ice loss. *Journal of Climate*, **29 (19)**, 6841–6859, doi:10.1175/JCLI-D-15-0651.1.

Vellinga, M., and R. Wood, 2002: Global climatic impacts of a collapse of the atlantic thermohaline circulation. *Climatic change*, **54**, 251–267.

Xiang, B., M. Zhao, I. Held, and J. Golaz, 2017: Predicting the severity of spurious 'double ITCZ'problem in CMIP5 coupled models from AMIP simulations. *Geophysical Research* , doi:10.1002/2016GL071992.

Zhang, L., and C. Wang, 2013: Multidecadal north atlantic sea surface temperature and atlantic meridional overturning circulation variability in CMIP5 historical simulations. *J. Geophys. Res.: Oceans*, **118**, 5772–5791, doi:10.1002/jgrc.20390.

Zhang, R., and T. Delworth, 2005: Simulated tropical response to a substantial weakening of the atlantic thermohaline circulation. *Journal of Climate*, doi:10.1175/JCLI3460.1.

Zhang, R., S. Kang, and I. Held, 2010: Sensitivity of climate change induced by the weakening of the atlantic meridional overturning circulation to cloud feedback. *Journal of Climate*, **23 (2)**, 378–389, doi:10.1175/2009JCLI3118.1.

LIST OF FIGURES

Fig. 1. Schematics of ITCZ shift damping mechanisms involved with (a, b) the subtropical cell, versus (c, d) the Atlantic meridional overturning cell. Red vertical arrows denote a hemispherically asymmetric top-of-atmosphere net radiative perturbation, and blue lines the associated zonal-mean overturning streamline responses. (Top) The subtropical cell (STC) and Hadley cell (HC) are mechanically coupled via zonal surface wind stress such that the STC and HC overturn in the same direction with similar response partitioning. In this limit a spinup of the STC (b) must associate with a spinup of the HC and enhanced demand from additional interhemispheric forcing. (Bottom) In contrast, the Atlantic Meridional Overturning Circulation (AMOC) is not subject to these constraints. A diverse set of response partitionings is possible. Even with no change in interhemispheric forcing a strengthening AMOC requires a weakening HC (c, d), or vice-versa, due to atmosphere-ocean competition for a fixed amount of required energy transport. That is, the two cells' responses can be prone to negatively covary. 28

Fig. 2. (a) Zonal-mean, annual-mean top-of-atmophere insolation perturbation (solid line) and net radiative flux responses (dotted line). (b): Zonal-mean, annual-mean precipitation responses. (c): Annual-mean cross-equatorial heat transport responses of total (grey), atmospheric (blue), and oceanic (brown)—control results are shown as a baseline. 29

Fig. 3. The decomposition of the annual-mean cross-equatorial total heat transport (HT_{eq}) responses. The HT_{eq} (black) is decomposed into heat transports due to clear-sky shortwave flux (blue), shortwave cloud radiative effect (CRE) (light blue), clear-sky longwave flux (red), longwave CRE (light red), and oceanic heat content trend. Δ means experiment minus control. All radiative fluxes are at the top of atmosphere. Averaging period is from model year 51 to 200. 30

Fig. 4. Scatter plot between the annual-mean cross-equatorial atmospheric heat transport (AHT_{eq}) response and annual-mean maximum meridional mass streamfunction response at the equator—as a proxy of Hadley circulation strength. Empty dots are 15-year running-averaged time-series for year 51–200 and the filled dots are the mean value of them. The strong relationship implies changes in gross moist stability across the experiments are not significant. 31

Fig. 5. The decomposition of the annaul-mean cross-equatorial atmospheric heat transport (green) into meridional mean circulation (orange) and eddy (blue) components. The eddy component include both stationary and transient eddies. 32

Fig. 6. Annual-mean, cross-equatorial oceanic heat transport (OHT) responses of global (a), Atlantic (b), and Pacific-Indian (c) ocean [unit: PW]. Different colors show different component of OHT: total (red), dynamic (light blue), thermodynamic (deep blue), and nonlinear (green). Yellow dots are for OHT normalized by basin width [unit: 10^{-7} PW / meter]. . . . 33

Fig. 7. Annual-mean overturning streamfunction responses for Atlantic (a) and Pacific-Indian basin (b). Right most panels are total response of control simulation [unit: Sv]. Warm (cold) colors are signed as clockwise (counter clockwise) circulations. Note that (a) and (b) have different depths and color bars. 34

Fig. 8. Time series of responses of AMOC strength(a), Atlantic cross-equatorial oceanic heat transport (b), Pacific-Indian asymmetric subtropical cell strength (c), and Pacific-Indian cross-equatorial oceanic heat transport (d). A solid line shows 5-year running mean and shading is ± one 5-year running standard deviation. AMOC strength is defined as a maximum over-

turning streamfunction within 30°N to 50°N latitude and 600m to 1400m depth in Atlantic. Pacific-Indian asymmetric subtropical cell strength is defined as a maximum of asymmetric component of overturning streamfunction within 7°N to 15°N latitude and 0m to 250m depth in Pacific-Indian. 35

Fig. 9. Scatter plots of annual-mean time series between tropical precipitation asymmetry index (PAI) and cross-equatorial oceanic heat transport (OHT) during Year 51 to 200. (top panels) long-term component defined as 15-year running average; (bottom panels) short-term component defined as anomalies from the long-term component. (a, d) Global ocean; (b, e) Atlantic ocean; (c, f) Pacific and Indian ocean. Regression lines for all experiments (grey) and for each experiment (color) are shown only for relationship whose r^2 is larger than 0.5. (g) shows correlation coefficients, r, of long-term (solid line) and short-term (dashed line) with different running mean windows. Zero running mean window means original time series. Errors bars are 95% confidence interval. 36

Fig. 10. Scatter plot between the annual-mean tropical precipitation asymmetry index (PAI) response and the annual-mean cross-equatorial atmospheric heat transport (AHT_{eq}) response. Empty dots are 15-year running-averaged time-series for year 51–200 and the filled dots are the mean value of them. 37

Fig. 11. Annual mean (a) surface temperature, (b) total cloud fraction, and (c) TOA shortwave cloud radiative effect responses (experiment minus control; except for CTRL) during years 51-200. . 38

Fig. 12. Annual-mean (a) $NEI_{eq}$and (b) AHT_{eq}. Errorbar is showing ±1 standard deviation of 15-year running-averaged time-series. The averaging period is year 51–200. 39

Fig. 13. Cross correlation between time series of Labrador Sea upper ocean (0–200m) density and Atlantic meridional overturning circulation (AMOC) strength, smoothed with a 5-year running mean, with negative values indicating Labrador Sea density leading. 40

Fig. 14. The hemispheric asymmetry of annual-mean tropical sea surface temperature (SST) near the equator calculated as the difference of mean SST [0°, 14.5°] minus mean SST [-14.5°, 0°] during years 51 to 200. 41

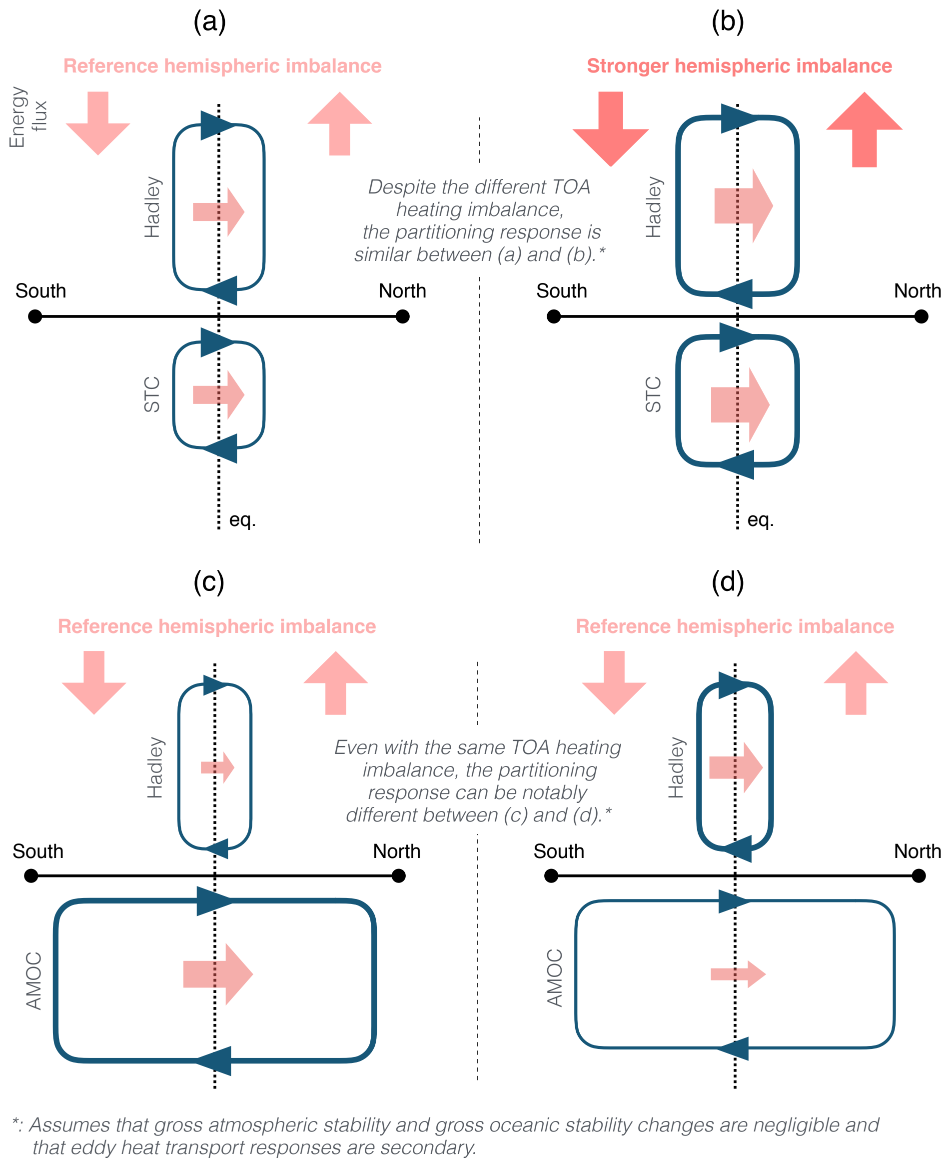

FIG. 1. Schematics of ITCZ shift damping mechanisms involved with (a, b) the subtropical cell, versus (c, d) the Atlantic meridional overturning cell. Red vertical arrows denote a hemispherically asymmetric top-of-atmosphere net radiative perturbation, and blue lines the associated zonal-mean overturning streamline responses. (Top) The subtropical cell (STC) and Hadley cell (HC) are mechanically coupled via zonal surface wind stress such that the STC and HC overturn in the same direction with similar response partitioning. In this limit a spinup of the STC (b) must associate with a spinup of the HC and enhanced demand from additional interhemispheric forcing. (Bottom) In contrast, the Atlantic Meridional Overturning Circulation (AMOC) is not subject to these constraints. A diverse set of response partitionings is possible. Even with no change in interhemispheric forcing a strengthening AMOC requires a weakening HC (c, d), or vice-versa, due to atmosphere-ocean competition for a fixed amount of required energy transport. That is, the two cells' responses can be prone to negatively covary.

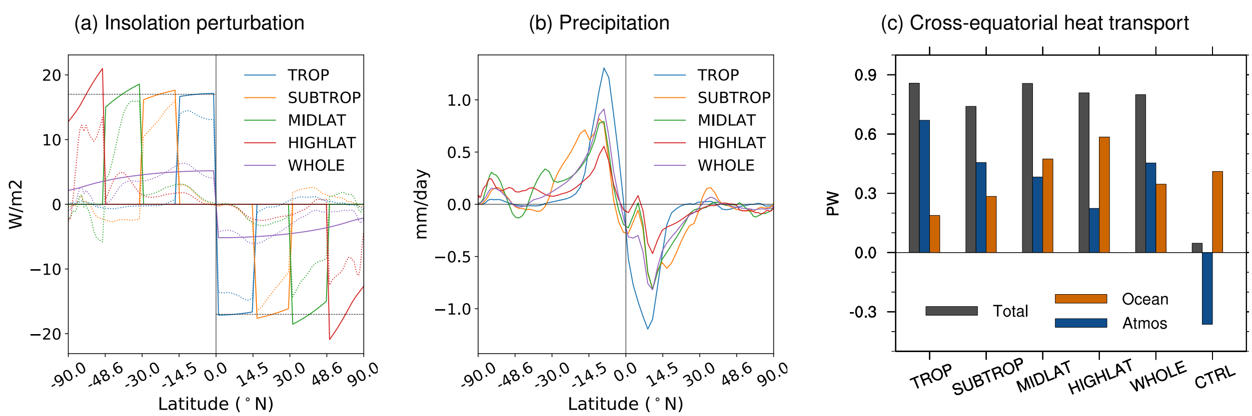

621 FIG. 2. (a) Zonal-mean, annual-mean top-of-atmophere insolation perturbation (solid line) and net radiative
622 flux responses (dotted line). (b): Zonal-mean, annual-mean precipitation responses. (c): Annual-mean cross-
623 equatorial heat transport responses of total (grey), atmospheric (blue), and oceanic (brown)—control results are
624 shown as a baseline.

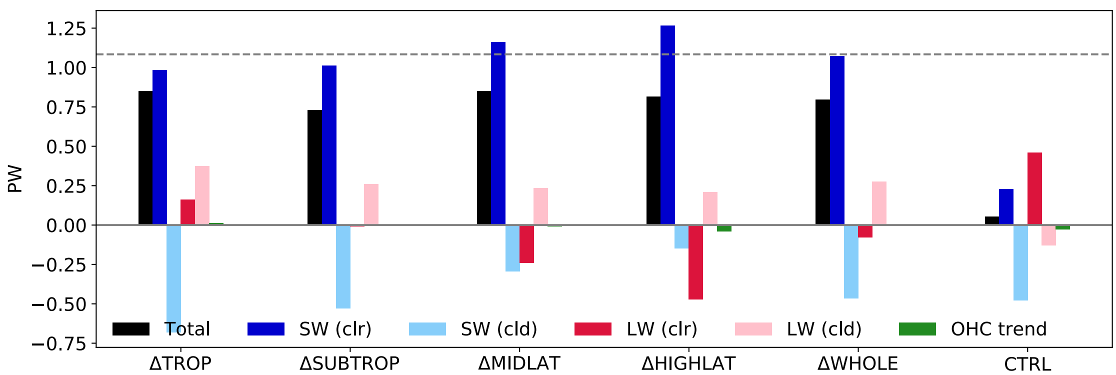

FIG. 3. The decomposition of the annual-mean cross-equatorial total heat transport (HT_{eq}) responses. The HT_{eq} (black) is decomposed into heat transports due to clear-sky shortwave flux (blue), shortwave cloud radiative effect (CRE) (light blue), clear-sky longwave flux (red), longwave CRE (light red), and oceanic heat content trend. Δ means experiment minus control. All radiative fluxes are at the top of atmosphere. Averaging period is from model year 51 to 200.

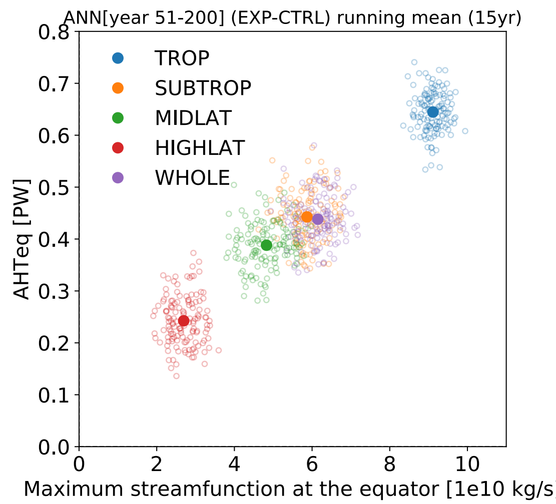

FIG. 4. Scatter plot between the annual-mean cross-equatorial atmospheric heat transport (AHT_{eq}) response and annual-mean maximum meridional mass streamfunction response at the equator—as a proxy of Hadley circulation strength. Empty dots are 15-year running-averaged time-series for year 51–200 and the filled dots are the mean value of them. The strong relationship implies changes in gross moist stability across the experiments are not significant.

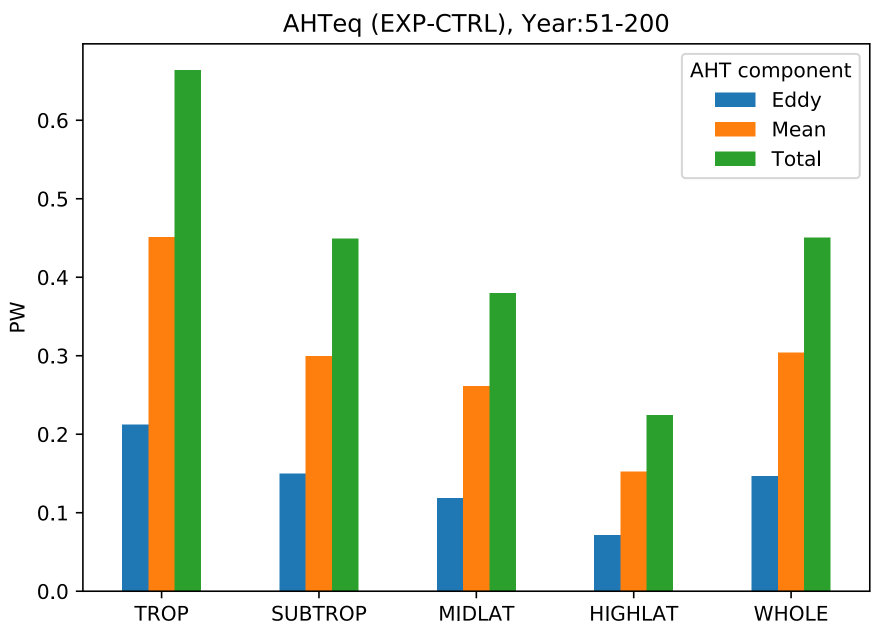

FIG. 5. The decomposition of the annaul-mean cross-equatorial atmospheric heat transport (green) into meridional mean circulation (orange) and eddy (blue) components. The eddy component include both stationary and transient eddies.

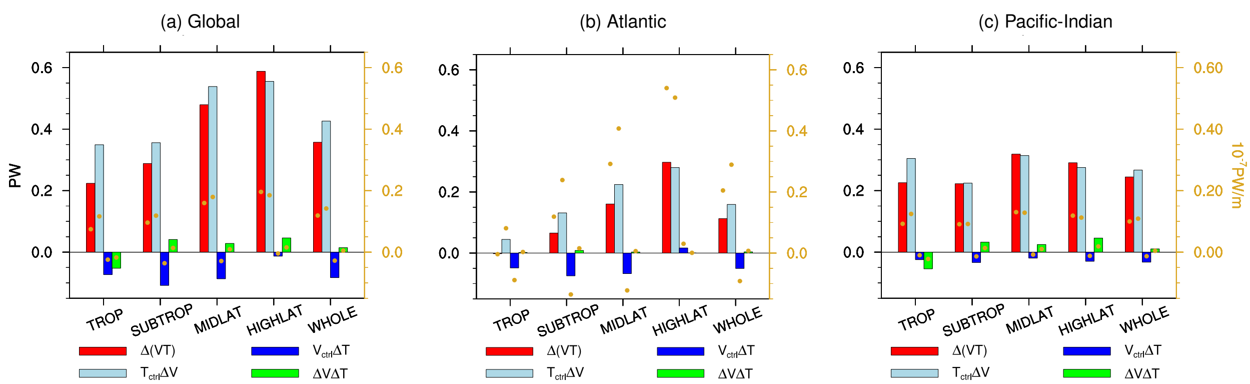

FIG. 6. Annual-mean, cross-equatorial oceanic heat transport (OHT) responses of global (a), Atlantic (b), and Pacific-Indian (c) ocean [unit: PW]. Different colors show different component of OHT: total (red), dynamic (light blue), thermodynamic (deep blue), and nonlinear (green). Yellow dots are for OHT normalized by basin width [unit: 10^{-7} PW / meter].

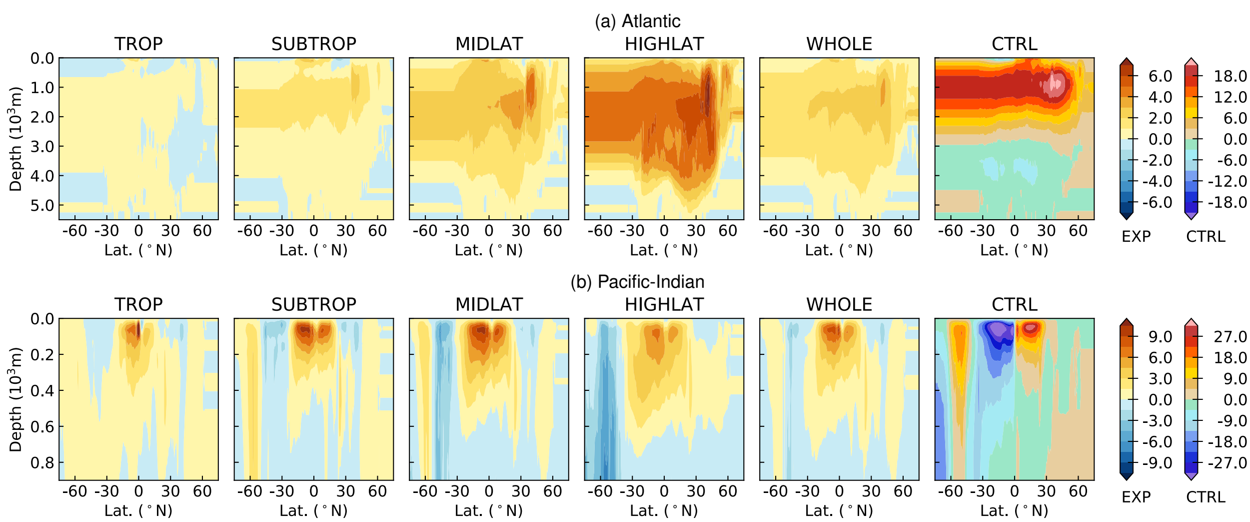

FIG. 7. Annual-mean overturning streamfunction responses for Atlantic (a) and Pacific-Indian basin (b). Right most panels are total response of control simulation [unit: Sv]. Warm (cold) colors are signed as clockwise (counter clockwise) circulations. Note that (a) and (b) have different depths and color bars.

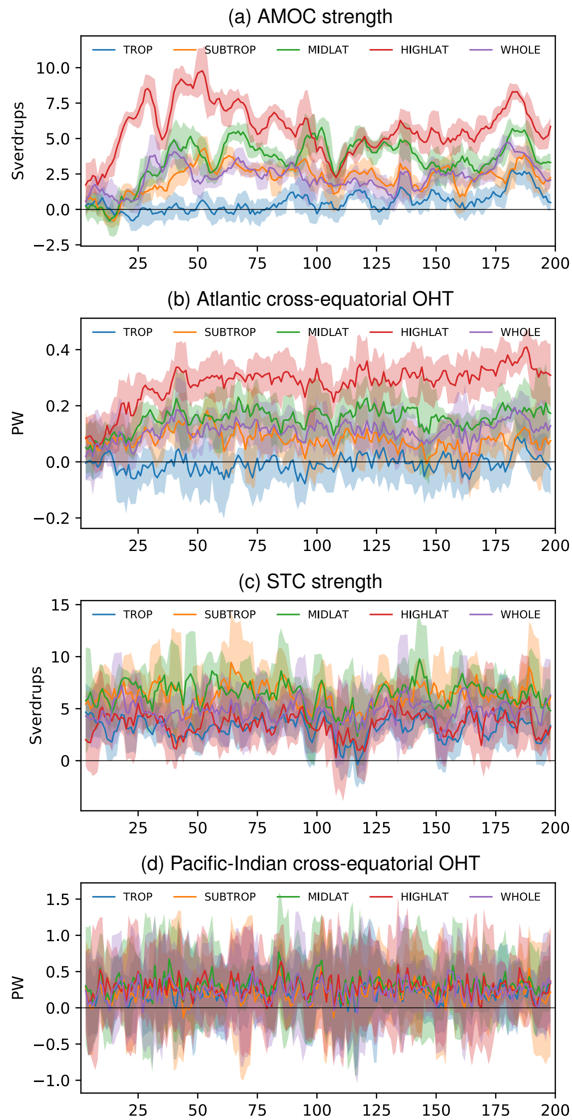

FIG. 8. Time series of responses of AMOC strength(a), Atlantic cross-equatorial oceanic heat transport (b), Pacific-Indian asymmetric subtropical cell strength (c), and Pacific-Indian cross-equatorial oceanic heat transport (d). A solid line shows 5-year running mean and shading is ± one 5-year running standard deviation. AMOC strength is defined as a maximum overturning streamfunction within 30°N to 50°N latitude and 600m to 1400m depth in Atlantic. Pacific-Indian asymmetric subtropical cell strength is defined as a maximum of asymmetric component of overturning streamfunction within 7°N to 15°N latitude and 0m to 250m depth in Pacific-Indian.

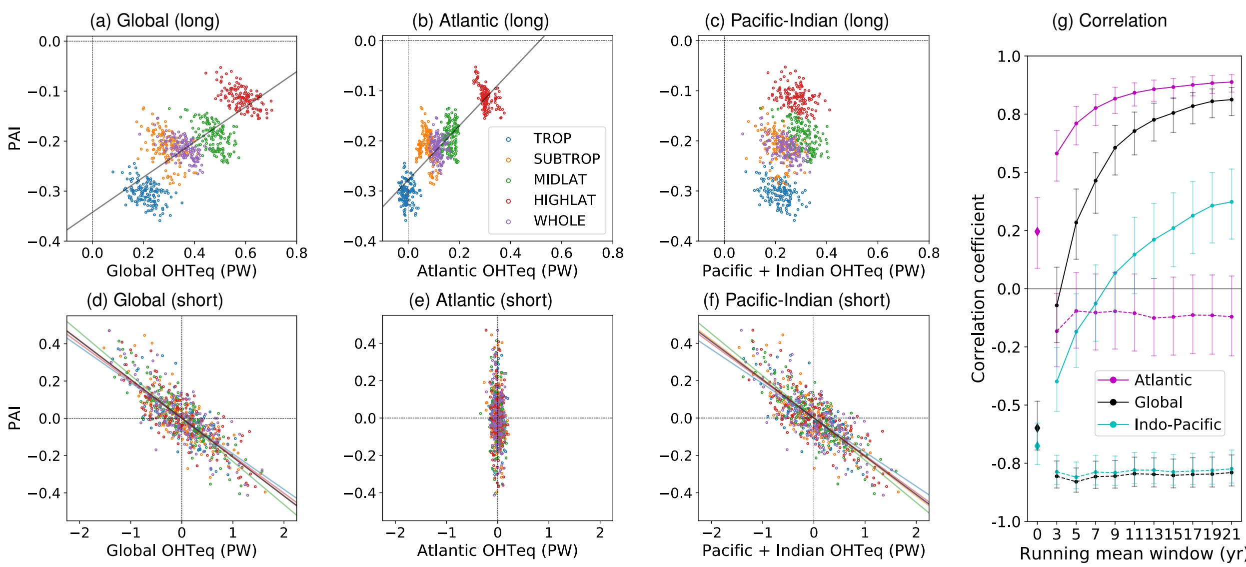

FIG. 9. Scatter plots of annual-mean time series between tropical precipitation asymmetry index (PAI) and cross-equatorial oceanic heat transport (OHT) during Year 51 to 200. (top panels) long-term component defined as 15-year running average; (bottom panels) short-term component defined as anomalies from the long-term component. (a, d) Global ocean; (b, e) Atlantic ocean; (c, f) Pacific and Indian ocean. Regression lines for all experiments (grey) and for each experiment (color) are shown only for relationship whose r^2 is larger than 0.5. (g) shows correlation coefficients, r, of long-term (solid line) and short-term (dashed line) with different running mean windows. Zero running mean window means original time series. Errors bars are 95% confidence interval.

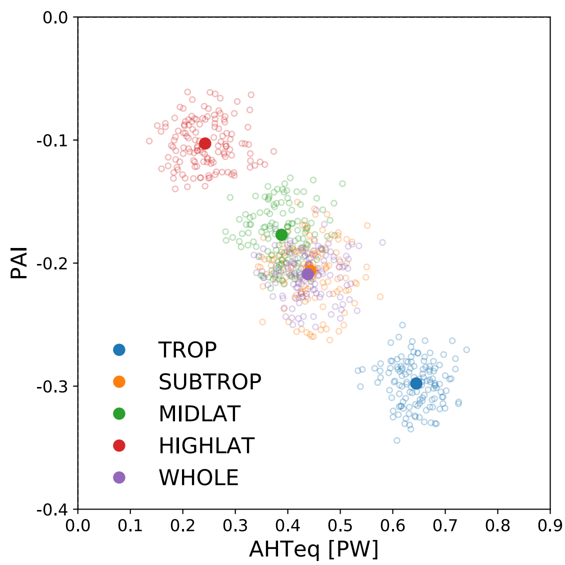

FIG. 10. Scatter plot between the annual-mean tropical precipitation asymmetry index (PAI) response and the annual-mean cross-equatorial atmospheric heat transport (AHT_{eq}) response. Empty dots are 15-year running-averaged time-series for year 51–200 and the filled dots are the mean value of them.

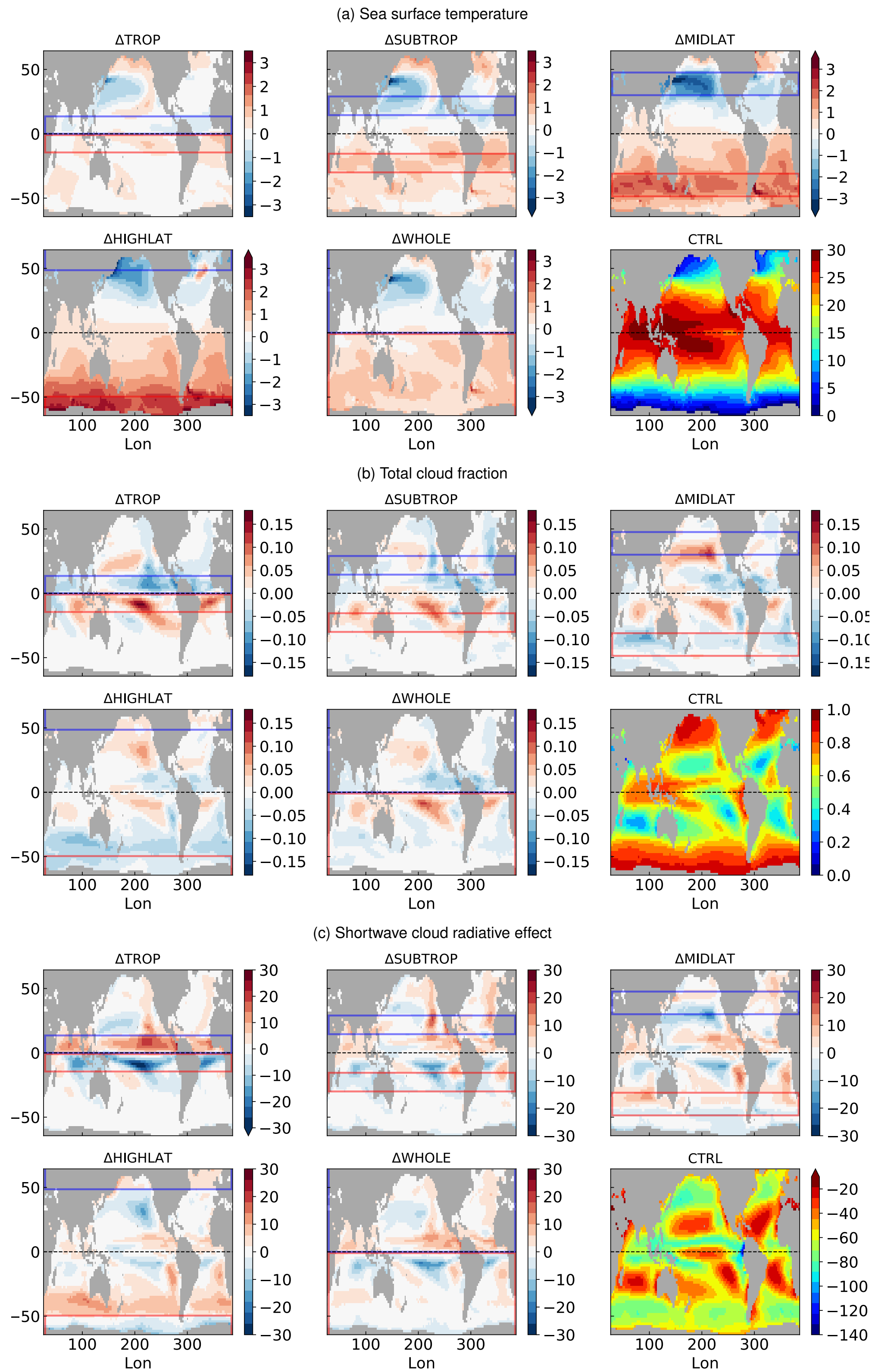

FIG. 11. Annual mean (a) surface temperature, (b) total cloud fraction, and (c) TOA shortwave cloud radiative effect responses (experiment minus control; except for CTRL) during years 51-200.

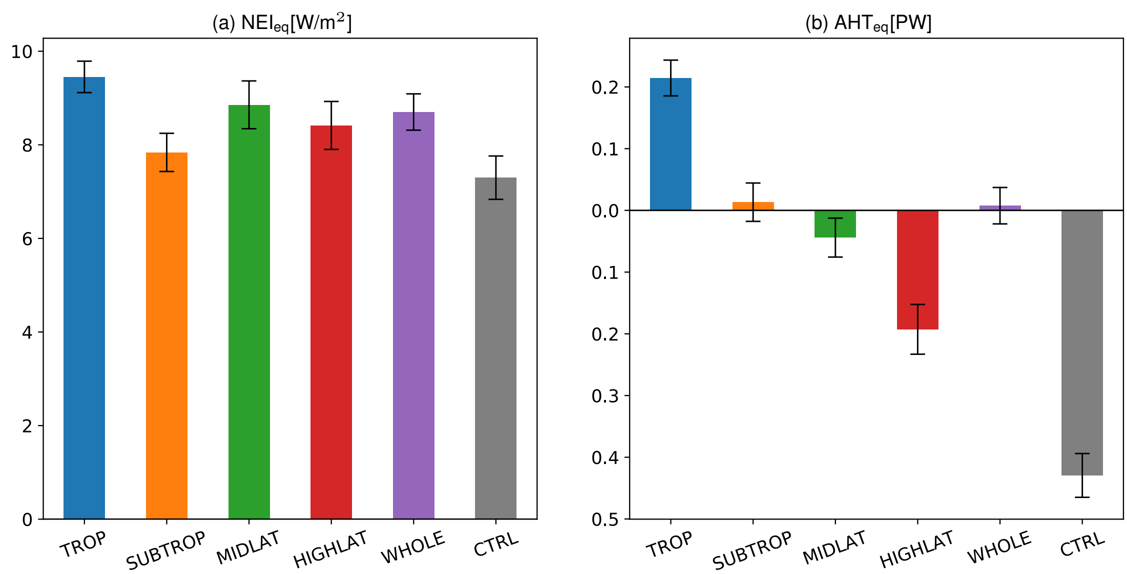

FIG. 12. Annual-mean (a) NEI$_{eq}$and (b) AHT$_{eq}$. Errorbar is showing ±1 standard deviation of 15-year running-averaged time-series. The averaging period is year 51–200.

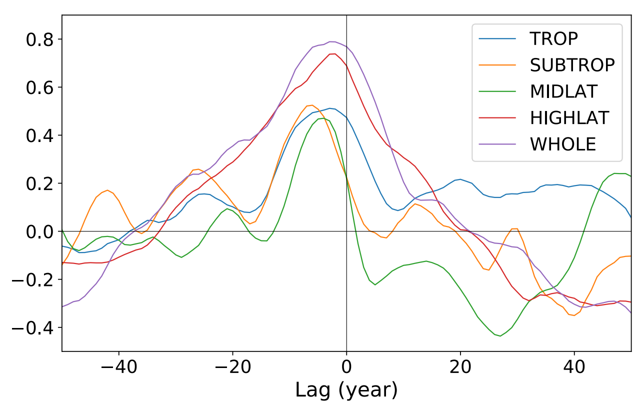

FIG. 13. Cross correlation between time series of Labrador Sea upper ocean (0–200m) density and Atlantic meridional overturning circulation (AMOC) strength, smoothed with a 5-year running mean, with negative values indicating Labrador Sea density leading.

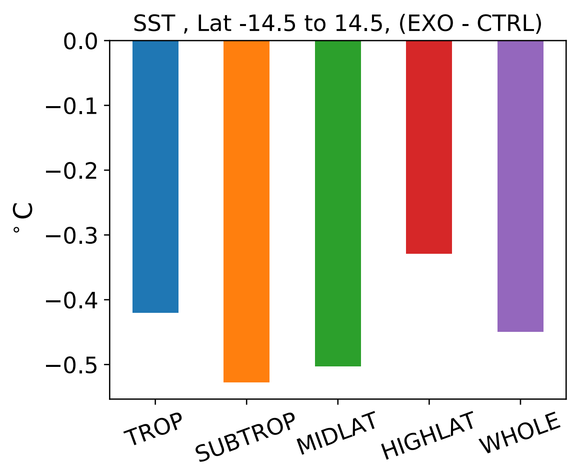

FIG. 14. The hemispheric asymmetry of annual-mean tropical sea surface temperature (SST) near the equator calculated as the difference of mean SST [0°, 14.5°] minus mean SST [-14.5°, 0°] during years 51 to 200.

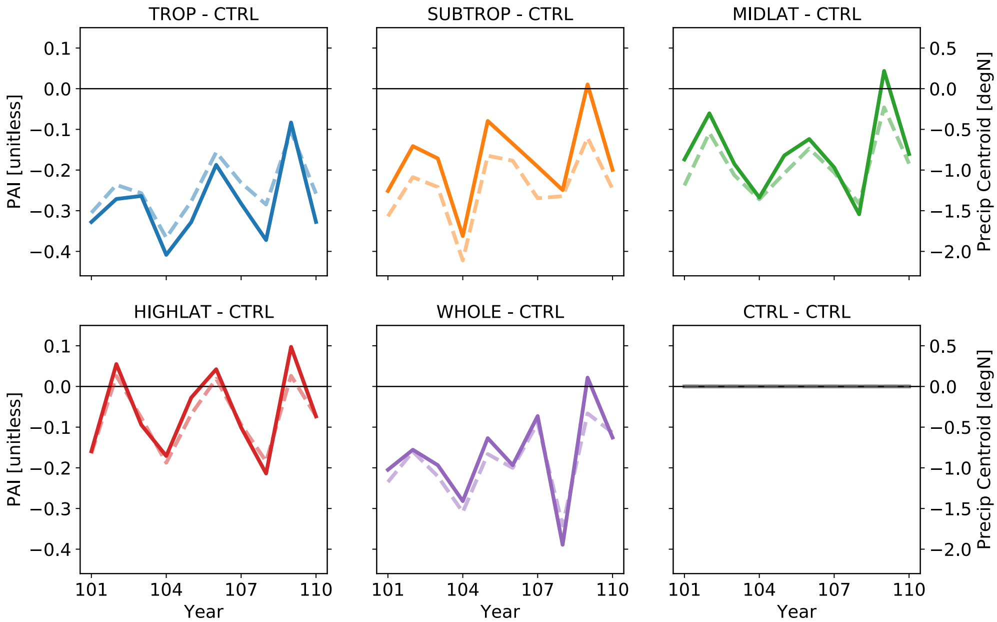

Supplemental Figutre S 1. Comparison between (solid) the precipitation asymmetry index and (dashed) precipitation centroid as alternate measures of the tropical rainfall responses, computed within 20 degrees of the equator, for an arbitrary time interval of the simulation (years 101-110).

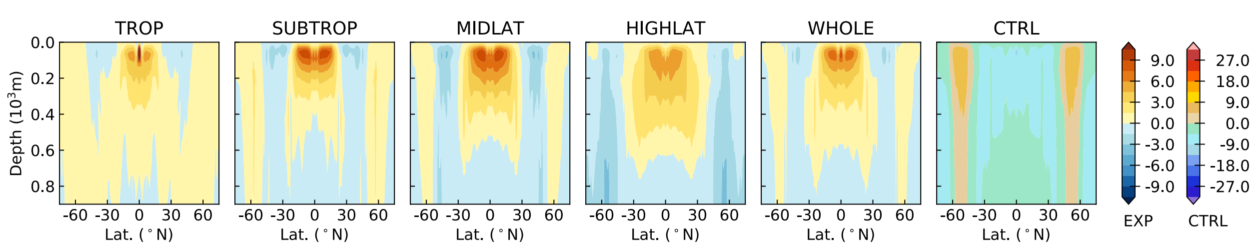

Supplemental Figutre S 2. Asymmetric component of figure 3b (Pacific-Indian meridional overturning streamfunction). Following Green and Marshall (2017, J. Climate), Asymmetric component is defined as $\psi(\phi) = [\psi(\phi) + \psi(-\phi)]/2$, where ψ is overturning streamfunction, and ϕ is latittude.

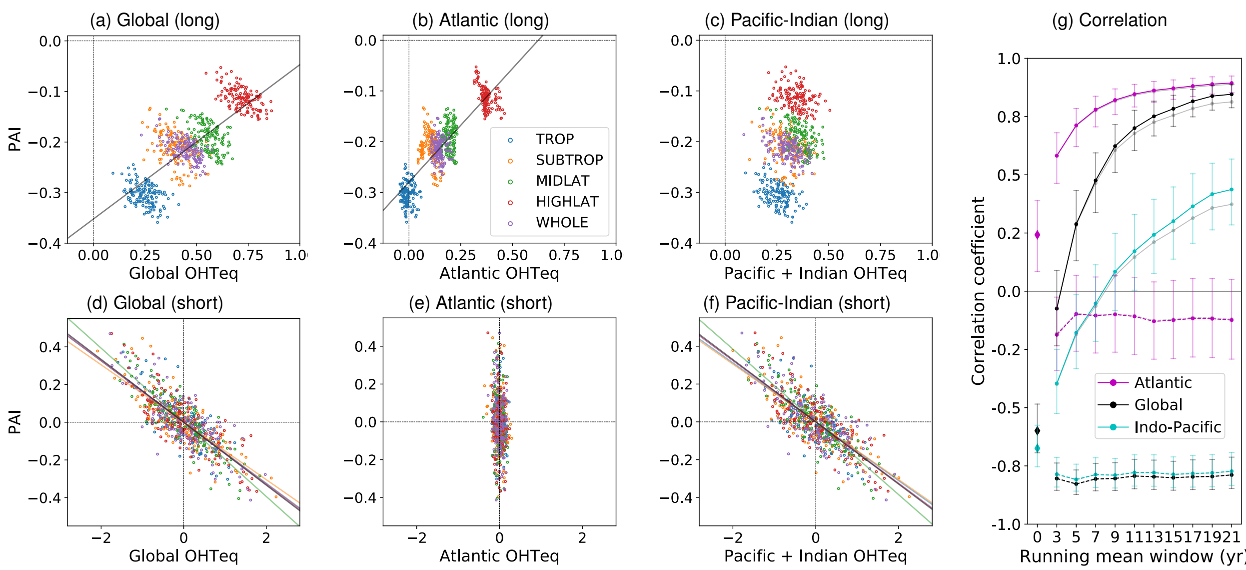

Supplemental Figutre S 3. Identical to Fig. 9 except that OHT_{eq}) responses are normalized by their respective total heat transport responses. The grey lines in (g) show the correlation coefficients before normalization, which are identical to those in Fig. 9g.